Interdisciplinary Research in Medical Sciences Specialty
ISSN: 3062-4401
2026, Volume 6, Issue 1, Page No: 178-193

Available online at: www.galaxypub.co/page/journals

Galaxy Publication

NAMPT-Driven Macrophage Polarization Regulates Smooth Muscle Cell Plasticity in Pulmonary Arterial Hypertension

Pieter Botha[1]*, Anel Van Wyk[1], Johan Marais[2]

[1]Department of Pulmonary Hypertension and Vascular Biology, Faculty of Medicine, Stellenbosch University, Stellenbosch, South Africa.
[2]Department of Macrophage Polarization and Smooth Muscle Biology, Faculty of Medicine, University of Pretoria, Pretoria, South Africa.

***E-mail** ✉ pieter.botha@sun.ac.za

Received: 01 February 2026; **Revised:** 24 April 2026; **Accepted:** 01 May 2026

ABSTRACT

Phenotypic modulation of smooth muscle cells (SMC) constitutes a central mechanism contributing to the development of pulmonary arterial hypertension (PAH). Despite its importance, the regulatory pathways involved are not yet fully understood. In this study, single-cell RNA sequencing was applied to pulmonary arterial tissues procured from lung transplant recipients to characterize cellular diversity and the transcriptomic signatures of major cell populations. Three separate SMC subpopulations were distinguished: contractile, fibroblast-like, and chondroid-like. Both trajectory inference and in vitro validation demonstrated a pronounced shift from the contractile toward the fibroblast-like phenotype in PAH. Intercellular communication analysis further uncovered classical (M1) macrophage polarization together with intensified pro-inflammatory interactions between macrophages and SMCs in diseased tissue. Nicotinamide phosphoribosyltransferase (NAMPT) was highlighted as a critical mediator of macrophage polarization. In Sugen/hypoxia (Su/Hx)-induced PAH mouse models, macrophages displayed upregulated Nampt expression, while its inhibition markedly reduced pro-inflammatory cytokine release. In co-culture experiments, targeted knockdown of Nampt in macrophages effectively prevented the transition of SMCs to a fibroblast-like state. Moreover, Ccl2/5 was identified as an essential cytokine driving SMC phenotypic changes. Taken together, this work provides a detailed cellular map of healthy human pulmonary arteries and establishes that NAMPT-orchestrated M1 macrophage polarization drives fibroblast-like phenotypic switching of SMCs through CCR2/CCR5-dependent intercellular signaling in PAH.

Keywords: Macrophage polarization, NAMPT, Phenotypic switching, Pulmonary arterial hypertension, Single-cell RNA sequencing, Smooth muscle cell

How to Cite This Article: Botha P, Van Wyk A, Marais J. NAMPT-Driven Macrophage Polarization Regulates Smooth Muscle Cell Plasticity in Pulmonary Arterial Hypertension. Interdiscip Res Med Sci Spec. 2026;6(1):178-93. https://doi.org/10.51847/1Qpu3bcA3T

Introduction

Pulmonary arterial hypertension (PAH) is a severe, relentlessly progressive, and presently incurable condition defined by extensive remodeling of the pulmonary arterioles, elevated pulmonary vascular resistance, and eventual right heart failure leading to death [1, 2], frequently requiring lung or heart-lung transplantation [3]. Excessive proliferation of pulmonary arterial smooth muscle cells (SMCs) is recognized as a fundamental process in disease advancement [4]. Although important progress has been achieved, the precise cellular and molecular underpinnings of PAH remain largely obscure, resulting in a clinical outlook more unfavorable than that of several malignancies [5].

SMCs play a pivotal role in vascular remodeling and exhibit considerable phenotypic plasticity, readily shifting from a contractile to a proliferative or synthetic phenotype. This transition is accompanied by increased production of non-contractile proteins such as fibronectin and vimentin, a process that is particularly prominent in PAH [6-10]. Inflammatory responses represent another key driver of PAH pathology, with macrophages and SMCs

collaborating to stimulate cell migration and growth via important chemokine pathways [11]. Nevertheless, the detailed mechanisms through which macrophages communicate with SMCs in the pulmonary vasculature are still poorly defined.

Nicotinamide phosphoribosyltransferase (NAMPT), also termed VISFATIN, functions as a rate-limiting enzyme in the NAD+ salvage pathway and has been linked to vascular remodeling in multiple cardiovascular disorders, including atherosclerosis, systemic hypertension, and PAH [12-14]. Prior research suggests that NAMPT influences endothelial cell and SMC behavior during pulmonary vascular remodeling in PAH [15, 16]; however, the complete mechanistic framework requires further clarification.

Utilizing single-cell RNA sequencing (scRNA-seq) on pulmonary arteries from both PAH patients and healthy controls, the present study documented fibroblast activation, macrophage M2 polarization, and SMC phenotypic diversity in non-diseased tissue. Side-by-side comparisons revealed amplified phenotypic switching of SMCs from contractile to fibroblast-like states within the neointimal layer in PAH. Examination of cell–cell interactions emphasized the significance of pro-inflammatory macrophage-SMC crosstalk and positioned NAMPT as a key inducer of M1 macrophage polarization. These findings were corroborated in mouse models, supporting their consistency and broader relevance. In addition, an in vitro co-culture model demonstrated that NAMPT-dependent M1 polarization in macrophages promotes fibroblast-like phenotypic conversion of SMCs via the CCR2/CCR5-NFκB signaling cascade.

Results and Discussion

Distinct activation patterns of vascular cells in healthy pulmonary arteries revealed through scRNA-seq

Pulmonary arteries affected by hypertension and corresponding non-diseased arteries from donors were procured during lung transplantation surgeries. These specimens were subjected to single-cell RNA sequencing (scRNA-seq) to delineate the cellular and molecular alterations associated with pulmonary arterial hypertension (PAH), **(Figure 1a)**.

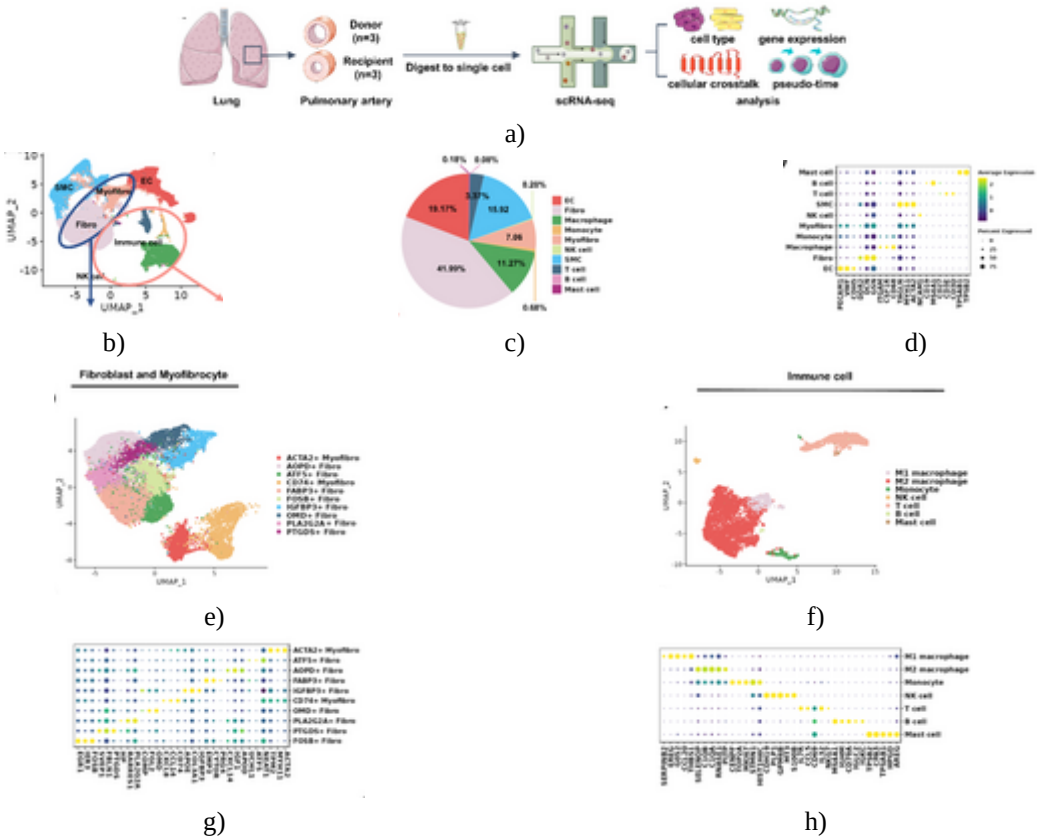

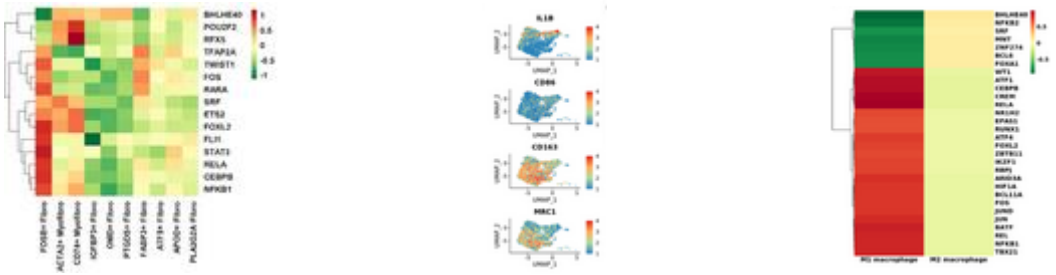

i) j) k)

Figure 1. Single-cell profiling of donor-derived cells, emphasizing fibroblast and immune cell subsets. (a) Overview of the study design, depicting the procurement of pulmonary artery specimens from lung transplant donors and recipients, followed by scRNA-seq analysis (n = 3 per group), tissue dissociation, data processing, and downstream computational evaluation. (b) UMAP visualization representing the major cell populations identified in donor samples. In total, 35,142 cells were integrated, revealing the following principal clusters: EC (endothelial cell), Fibro (fibroblast), Macrophage, Monocyte, Myofibro (myofibrocyte), NK cell, SMC (smooth muscle cell), and T cell. Fibroblasts and myofibrocytes (indicated by the blue circle) underwent further subclustering and are displayed in panel (e), whereas immune cells (marked by the red circle) are shown in panel (h). (c) Relative abundance of each identified cluster. (d) Dot plot highlighting canonical marker genes for the main cell populations, where dot diameter corresponds to the proportion of expressing cells within a cluster and color intensity reflects average expression levels. (f) Dot plot illustrating the three most distinctive marker genes for each fibroblast and myofibrocyte subpopulation. (g) Heatmap of transcription factor (TF) activity scores, computed with the DoRothEA R package, showcasing the 15 most variably active TFs across the ten fibroblast and myofibrocyte subclusters. (i) Dot plot displaying the five most highly differentially expressed genes per immune cell subpopulation. (j) Key marker genes employed for cell type annotation, encompassing established indicators of M1 macrophages (IL1B and CD86) and M2 macrophages (CD163 and MRC1). (k) Heatmap illustrating transcription factor (TF) activity patterns in M1 and M2 macrophage populations. Portions of the figure were created with Servier Medical Art (http://smart.servier.com/), used under a Creative Commons Attribution 3.0 unported license. scRNA, single-cell RNA sequencing; SMC, smooth muscle cells.

Owing to the limited prior exploration of this tissue, earlier transcriptomic investigations have predominantly examined selected cell populations such as endothelial cells or smooth muscle cells [17, 18]. The present work therefore aimed to generate a more holistic portrait of the gene expression landscape across human pulmonary arteries. From three donors, 35,142 individual cells were profiled and assigned to six primary categories using well-established lineage-specific markers (stromal compartment: PECAM1+ endothelial cells, MYH11+ smooth muscle cells, DCN+ fibroblasts; immune compartment: CD68+ monocytes/macrophages, CD3D+ T cells, NCAM1+ NK cells). Stromal cells accounted for the majority of the profiled population **(Figures 1b–1d)**.

Within the pulmonary artery wall, fibroblasts and myofibrocytes emerged as the predominant populations, comprising roughly 49.1% of all cells **(Figure 1c)**. Unsupervised clustering based on unique transcriptional signatures further resolved these into eight fibroblast subclusters and two myofibrocyte subclusters **(Figure 1e)**. Analysis of defining differentially expressed genes (DEGs), transcription factor profiles, gene ontology (GO) enrichment, and Kyoto Encyclopedia of Genes and Genomes (KEGG) pathway annotations uncovered specialized functional roles. Specifically, FABP3+, APOD+, and PLA2G2A+ fibroblasts were implicated in lipid handling, the OMD+ subpopulation showed associations with bone metabolism, and FOSB+ fibroblasts participated in stress adaptation via upregulation of MAPK, JAK/STAT, and NF-κB cascades **(Figures 1f and 1g)**. The IGFBP3+ fibroblasts likely represent a transitional population en route to myofibrocyte differentiation, given their proximity to myofibrocytes and enrichment for vascular smooth muscle contraction pathways. Notably, myofibrocytes were identified even in non-diseased arteries; these cells expressed supplementary contractile elements and actin-related proteins and separated into ACTA2+ and CD74+ groups. CD74+ myofibrocytes strongly expressed inflammatory mediators, including CXCL8, CCL14, and CD74, indicative of responses to hypoxic or stressful conditions. ACTA2+ myofibrocytes, on the other hand, elevated genes governing contractility (such as ACTG2, TAGLN, and TPM2) and may contribute to vascular disorders including aortic aneurysm/dissection and PAH. Intriguingly, these cells also displayed signatures suggestive of thermosensory functions and potential influence on epithelial

proliferation **(Figure 1e)**. Transcription factor activity was generally comparable across myofibrocyte subclusters, with the exception of elevated RFX5 and POU2F2 in CD74+ cells, consistent with roles in antigen presentation and T lymphocyte regulation [19, 20] **(Figure 1g)**.

Macrophage polarization in the pulmonary artery

Subsequent examination of six principal immune cell populations in healthy pulmonary arteries revealed that myeloid cells—chiefly macrophages (~71.1%)—represented the dominant immune compartment. These macrophages could be subdivided into M1 and M2 subtypes **(Figure 1h)**. Analysis of differentially expressed genes across cell clusters illustrated substantial heterogeneity within these populations **(Figure 1i)**. M1 macrophages were distinguished by IL1B expression together with transcription factors such as JUN, FOS, NFKB1 and RUNX1, aligning with their pro-inflammatory role. By comparison, M2 macrophages comprised 89.1% of the total macrophage pool and were identified by CD163+ and MRC1 (CD206)+ markers. They additionally expressed transcription factors including ZNF274, BCL6 and FOXA1, consistent with anti-inflammatory and reparative functions [21] **(Figures 1j and 1k)**.

Altered smooth muscle cell phenotypes in the pulmonary artery

Pulmonary arterial smooth muscle cells were resolved into eight distinct sub-clusters **(Figure 2a)**. Application of canonical phenotype-specific markers—contractile (MYH11, CNN1), fibrotic (DCN), and chondroid (BMP2)—enabled classification of the cells into contractile SMCs, fibroblast-like SMCs, and chondroid-like SMCs **(Figures 2b and 2c)**. Transcriptional profiling and pathway enrichment analyses confirmed unique molecular signatures and functional attributes associated with the chondroid-like and fibroblast-like SMC populations. Furthermore, elevated levels of JUN, RELB, STAT1, NFKB1 and SMAD3 in the switched SMC phenotypes pointed to engagement of the JAK/STAT, NF-κB, and PI3K/Akt signaling cascades **(Figures 2d and 2e)**.

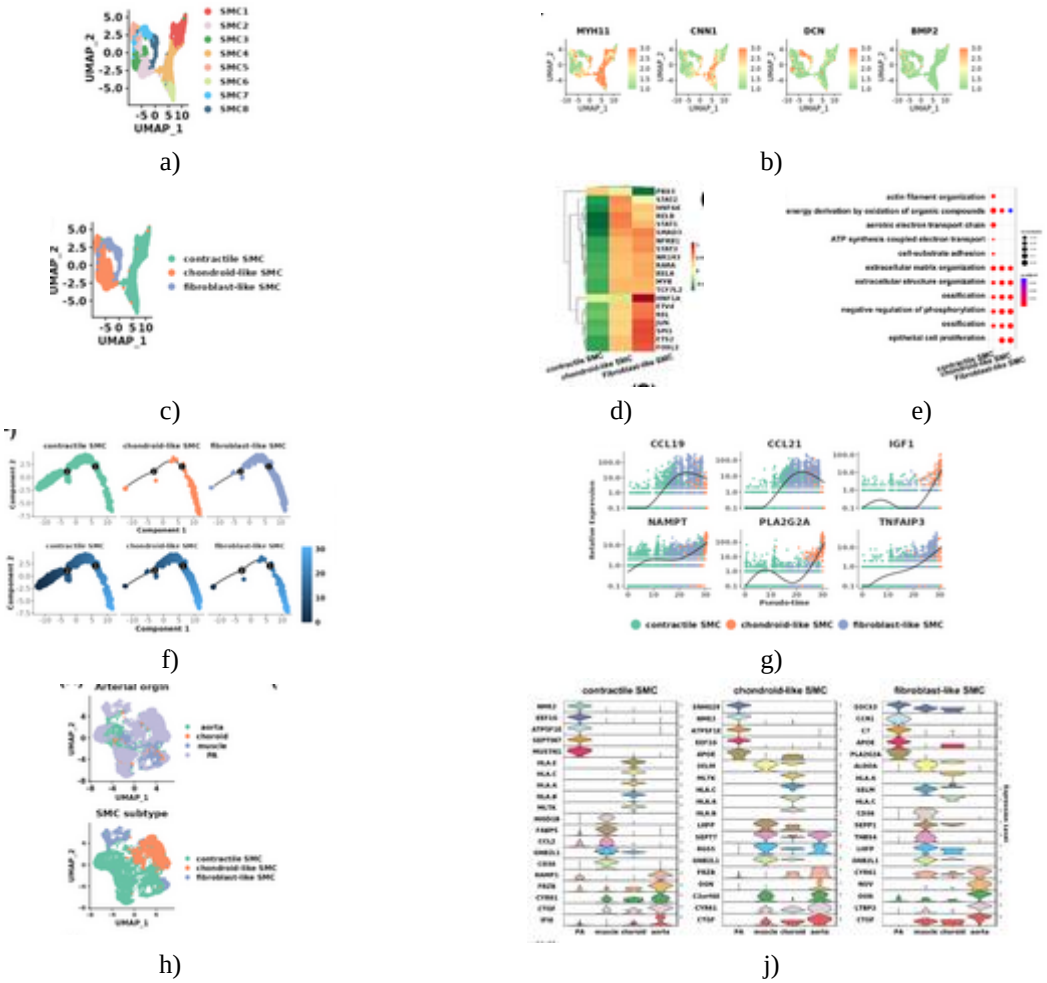

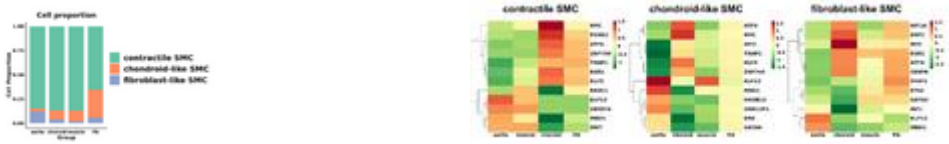

i) k)

Figure 2. Heterogeneity of Smooth Muscle Cells in the Human Pulmonary Artery.
(a) UMAP visualization depicting the partitioning of smooth muscle cells into eight separate clusters (SMC1–SMC8). (b) Feature plots illustrating the spatial distribution of key marker genes corresponding to the contractile phenotype (MYH11 and CNN1), fibroblast-like phenotype (DCN), and chondroid-like phenotype (BMP2), with expression intensity indicated by color scale overlaid on the UMAP embedding. (c) Assignment of smooth muscle cells to contractile smooth muscle cells (SMCs), chondroid-like smooth muscle cells (C-SMCs), and fibroblast-like smooth muscle cells (F-SMCs) on the basis of their transcriptional profiles, shown in the UMAP representation. (d) Heatmap presenting the inferred activities of transcription factors (TFs) in contractile SMCs, chondroid-like SMCs, and fibroblast-like SMCs. (e) Dot plot summarizing Gene Ontology (GO) pathway enrichment results, emphasizing the leading differentially enriched biological processes identified from genes differentially expressed among contractile SMCs, chondroid-like SMCs, and fibroblast-like SMCs. (f) Pseudotime trajectory reconstruction of smooth muscle cell subsets, color-labeled by cell subtype (upper-left panel) and developmental progression along pseudotime (upper-right panel). The accompanying density plot (lower panel) illustrates the overall distribution of smooth muscle cells throughout the pseudotime continuum. (g) Dynamic expression patterns of representative genes across the pseudotime axis. (h) Integrated UMAP projection of smooth muscle cells originating from several tissues, annotated by tissue source (upper panel) and cell subtype (lower panel). (i) Bar graph comparing the relative abundance of smooth muscle cells in each examined tissue. (j) Violin plots highlighting the expression of the five most differentially expressed genes for contractile SMCs, chondroid-like SMCs, and fibroblast-like SMCs across the studied tissues. (k) Heatmap comparing transcription factor (TF) activity profiles for contractile SMCs, chondroid-like SMCs, and fibroblast-like SMCs from multiple tissues. C-SMCs, chondroid-like smooth muscle cells; F-SMCs, fibroblast-like smooth muscle cells; GO, gene ontology; SMC, smooth muscle cells; TF, transcription factor.

Tracing the phenotypic transition trajectory of SMCs demonstrated that chondroid-like SMCs occupied the endpoint of the continuum, while fibroblast-like SMCs represented an intermediate stage in the switching process **(Figure 2f)**. The chemokines CCL19 and CCL21 were implicated in driving the progression from contractile SMCs to fibroblast-like SMCs, although their levels declined during the shift toward chondroid-like SMCs. Of particular interest, the continuous high expression of NAMPT pointed to its critical involvement in regulating SMC phenotype modulation **(Figure 2g)**.

Comparative examination across arteries further underscored the specialized composition of smooth muscle cells in the pulmonary artery. Under non-diseased conditions, chondroid-like SMCs reached their highest proportion in the pulmonary artery (28.8%), in contrast to the aorta, which showed the largest share of fibroblast-like SMCs (12.2%) **(Figures 2h and 2i)**. Genes including ATP5F1E, NME2, EEF1G, and PLA2G2A exhibited elevated expression, characterizing a tissue-specific transcriptional profile unique to pulmonary arterial SMCs **(Figure 2j)**. Additional transcriptional and functional enrichment analyses linked MYC, ATF6, and HIF1A to the distinctive properties of these cells, particularly in relation to cellular stress responses, oxidative metabolic processes, and PAH-associated mechanisms **(Figure 2k)**.

Fibroblast-like phenotypic transition of neointimal SMCs in PAH

Smooth muscle cells possess the capacity to shift between contractile and synthetic states when exposed to a range of environmental triggers and external signals [10, 18]. To investigate this process in PAH, the molecular and cellular characteristics of SMC phenotypic switching were systematically profiled. By combining single-cell transcriptomic datasets from both diseased (hypertensive) and healthy pulmonary arteries, ten major cell populations were delineated. Within this framework, smooth muscle cells were resolved into contractile, fibroblast-like, and chondroid-like subtypes using established marker genes **(Figures 3a and 3b)**. PAH conditions

were associated with a pronounced rise in the fibroblast-like SMC population alongside a reduction in chondroid-like SMCs **(Figure 3a)**.

Gene expression comparisons indicated enhanced pro-inflammatory and pro-contractile activities in both contractile SMCs and fibroblast-like SMCs derived from hypertensive arteries. These changes were marked by the increased transcription of several genes, notably IGFBP2, XIST, TNFRSF12A, JUNB, ACTA2, ACTC1, and RGS5. Pseudotime analysis reconstructed the directional transition from contractile SMCs toward fibroblast-like or chondroid-like states, revealing an amplified tendency for fibroblast-like differentiation during PAH development **(Figures 3c and 3d)**. Along this trajectory, cytokine expression patterns highlighted the progressive loss of the contractile identity, emergence of fibroblast-like and stressed phenotypes, and the contributory roles of NFκB and TGF-β/SMAD signaling in driving the fibroblast-like phenotypic switch **(Figure 3e)**.

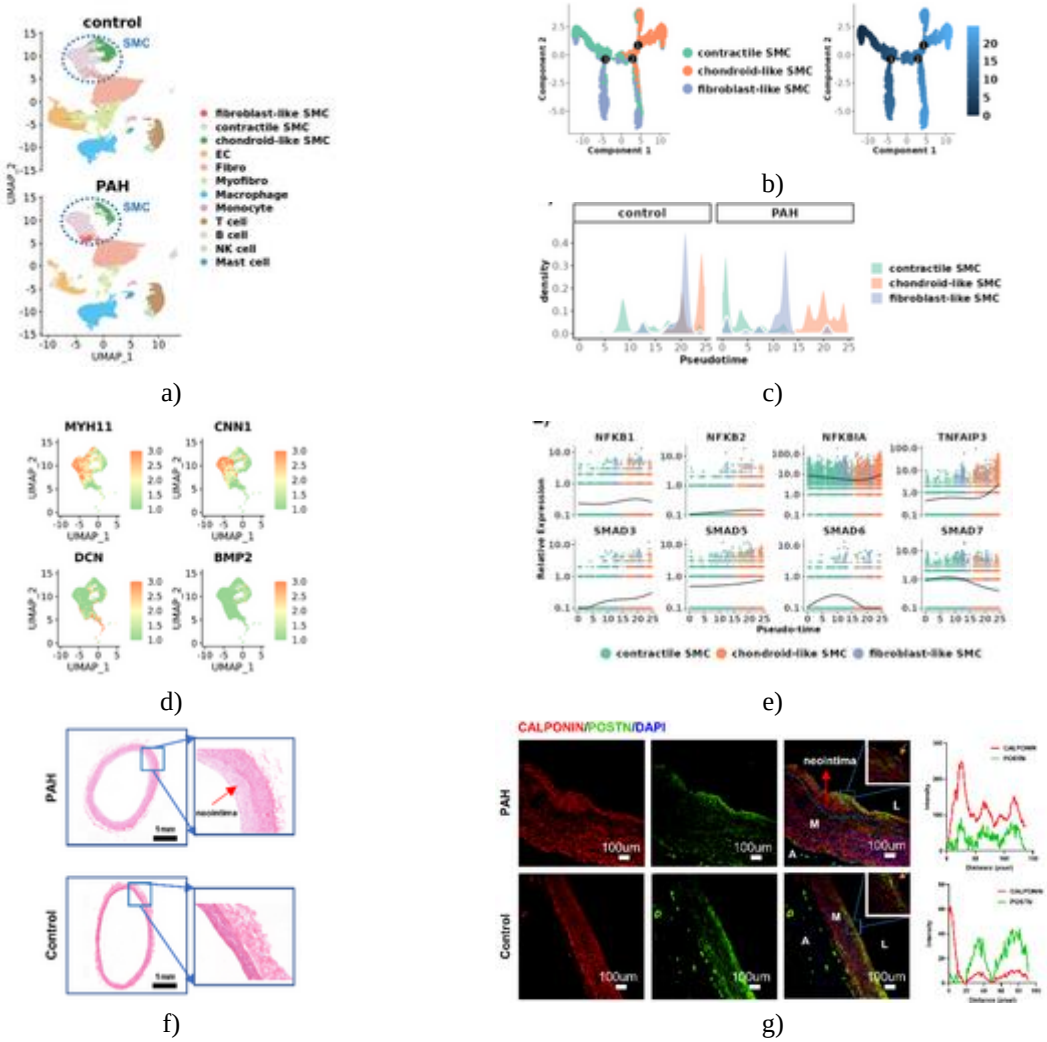

Figure 3. Smooth Muscle Cell Phenotypic Switching in Pulmonary Arterial Hypertension. (a) UMAP plots displaying the cellular landscape of pulmonary arterial cells in control specimens (upper panel) and PAH specimens (lower panel). (b) Canonical marker genes applied for cell type annotation, including well-established indicators for the contractile phenotype (MYH11 and CNN1), fibroblast-like phenotype (DCN), and chondroid-like phenotype (BMP2). (c) Pseudotime trajectory mapping of smooth muscle cell populations, color-coded according to cell subtype (left panel) and developmental progression along pseudotime (right panel). (d) Density distribution illustrating the positioning of the entire smooth muscle cell population from control and PAH conditions across the pseudotime axis. (e) Temporal expression dynamics of selected genes along the pseudotime trajectory. (f) Hematoxylin-eosin (HE) staining images of healthy and hypertensive pulmonary arteries (scale bar, 1 mm), with enlarged views of the blue-highlighted areas. The neointima formation in hypertensive arteries is highlighted by a red arrow. (g) Immunofluorescence staining of representative normal and hypertensive arterial sections (scale bar, 100 μm).

Key vascular compartments are denoted as L (lumen), M (media), and A (adventitia). Insets show magnified regions outlined in blue, where the blue dashed line and red arrows delineate the neointimal layer. The line plot on the right displays intensity profiles reflecting co-localization at the position marked by the orange arrow. A, adventitia; L, lumen; M, media.

Further histological and immunofluorescence analyses revealed pronounced neointimal hyperplasia accompanied by the presence of CALPONIN+ POSTN+ fibroblast-like SMCs within the neointimal layer of hypertensive pulmonary arteries. These cells were particularly enriched in the innermost region adjacent to the lumen, supporting their contribution to vascular remodeling. Such features were rarely observed in healthy vessels **(Figures 3f and 3g)**. Collectively, these observations suggest that in PAH, arterial SMCs undergo a fibroblast-like phenotypic transition within the neointima, potentially contributing to progressive lumen narrowing and obstruction.

NAMPT-driven macrophage M1 polarization promotes SMC phenotypic switching

Given the established involvement of phenotypic modulation of SMCs in various vascular disorders, the study next explored alterations in inflammatory signaling networks by analyzing ligand-receptor interactions. Cellular communication networks were substantially enhanced in PAH, with particularly strong inflammatory crosstalk between macrophages and both contractile SMCs and fibroblast-like SMCs. This was evidenced by markedly increased incoming and outgoing interaction strengths, highlighting their central contribution to disease advancement. In contrast, chondroid-like SMCs exhibited comparatively limited intercellular signaling activity **(Figure 4a)**. Moreover, macrophages in PAH displayed significantly heightened activation of pro-inflammatory signaling pathways, such as CCL, TNF, IL1, IL6, and IL16, along with several growth factor-mediated cascades including FGF, VEGF, PDGF, IGF, EGF, and HGF **(Figure 4b)**.

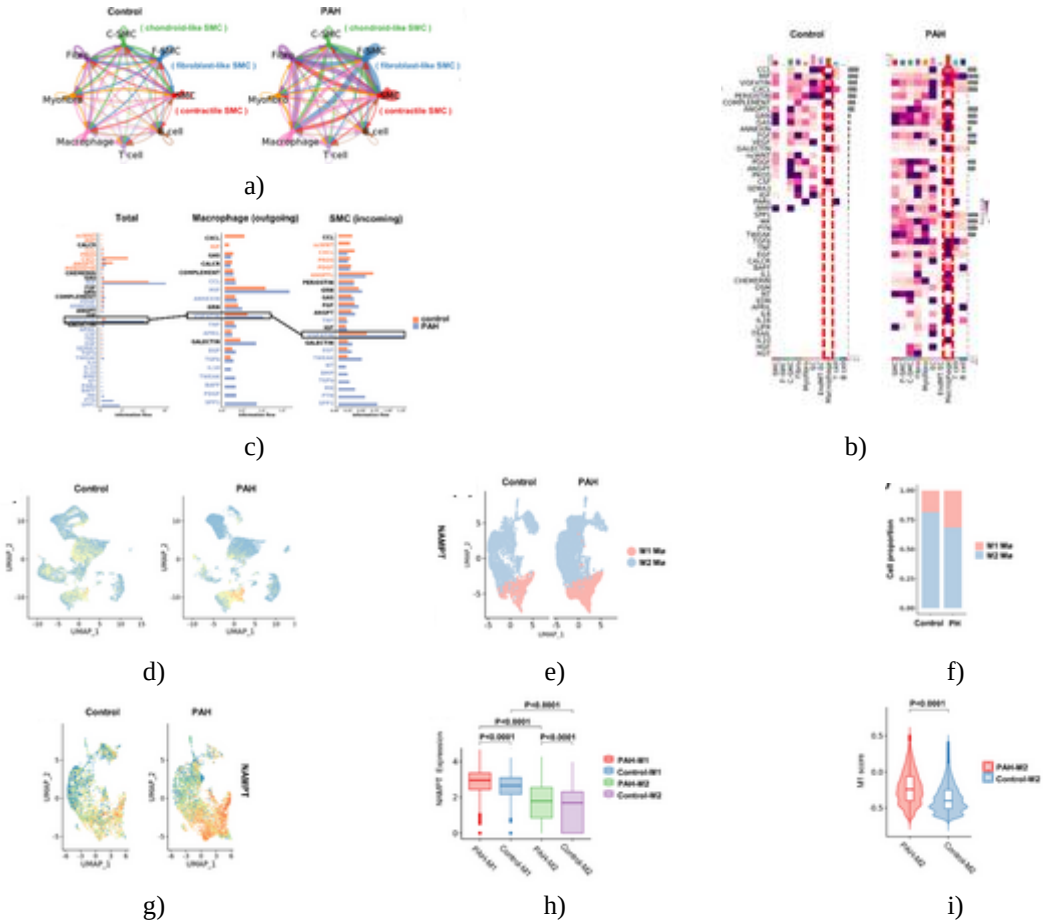

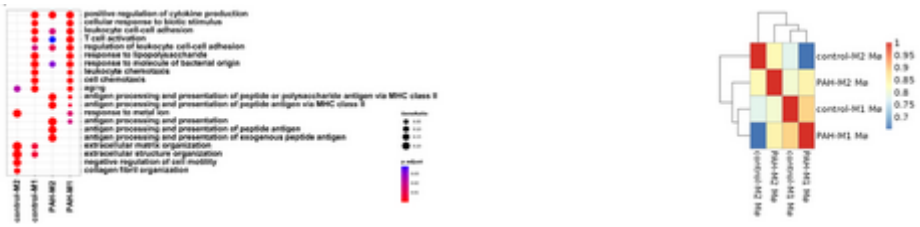

j) k)

Figure 4. Macrophage Upregulation of NAMPT Expression Drives M1 Polarization in PAH. (a) Circle diagrams illustrating both the quantity and intensity of ligand-receptor interactions among the eight major cell populations in control versus PAH specimens. (b) Heatmap representing the comparative activity levels of various signaling networks across clusters, with the macrophage signaling signature prominently outlined by a red dashed rectangle. (c) Ordering of signaling pathways by the density of information flow for macrophage-secreted signals and smooth muscle cell-received inputs in the control and PAH cohorts. (d) UMAP embedding highlighting NAMPT transcript distribution throughout pulmonary arterial cells. Macrophages were isolated for in-depth examination in subsequent panels. (e) UMAP projection of macrophage subsets from control and PAH tissues, annotated as M1 (red) or M2 (blue) subtypes based on characteristic marker profiles. (f) Bar chart quantifying the relative abundance of M1 and M2 macrophage populations. (g) UMAP display of NAMPT expression specifically in macrophages, demonstrating upregulation in PAH samples and preferential association with the M1 phenotype across both conditions. (h) Boxplot summarizing NAMPT expression differences between M1 and M2 macrophages in control and PAH groups. The plot displays the interquartile range (IQR) as boxes, the median as a central line, and whiskers extending to 1.5 × IQR, with individual outliers shown as points. Statistical significance between groups was evaluated using Student's t-test. (i) Violin plot depicting the distribution of M1 phenotype scores within M2 macrophages from control and PAH samples. Significant differences were confirmed by Student's t-test. (j) Dot plot of Gene Ontology (GO) enrichment results, identifying key biological pathways significantly overrepresented among differentially expressed genes in M1 and M2 macrophages under control and PAH conditions. (k) Inter-population correlation analysis of macrophage subsets. Genes with the greatest variance were selected from each population, followed by assessment of linear relationships via Pearson correlation coefficients. GO, gene ontology.

Notably, VISFATIN (also designated NAMPT), a pro-inflammatory adipokine implicated in systemic insulin resistance and dyslipidemia, displayed substantially amplified information flow within the PAH cohort. This increase was most evident in the macrophage-SMC communication axis **(Figure 4c)**. As anticipated, targeted assessment of NAMPT transcript abundance across pulmonary arterial cells identified prominent enrichment specifically within macrophages **(Figure 4d)**.

After isolating and re-clustering the macrophage population, NAMPT expression was found to be preferentially elevated in M1 macrophages relative to their M2 counterparts **(Figures 4e and 4g)**. Subtype assignment relied on conventional M1/M2 signature genes and associated biological processes **(Figure 4j)**. NAMPT levels were significantly higher in both macrophage subtypes in PAH compared to control samples **(Figures 4g and 4h)**. Consistent with the expanded M1 fraction, application of a classical M1 gene signature [22] to M2 macrophages indicated a shift toward M1 characteristics in the disease state **(Figures 4f and 4i)**.

Correlation profiling revealed that M2 macrophages isolated from PAH tissues exhibited gene expression patterns more akin to M1 cells than to control M2 cells, lending further support to this phenotypic convergence **(Figure 4k)**. Supplementary enrichment analyses implicated NFκB/TNFα signaling as a key pathway in M1 macrophages. Taken together, the data suggest that NAMPT upregulation enhances M1 polarization of macrophages, thereby contributing to the adoption of a fibroblast-like state by SMCs in PAH.

Hypoxia-induced macrophage nampt upregulation is associated with SMC phenotypic transition in mice

To confirm the validity of this mechanism, single-cell RNA sequencing data from mouse pulmonary arteries were obtained from the GEO repository (accession number GSE210248). After quality control and integration, 9201 cells were re-grouped according to their transcriptional signatures and sample annotations, consisting of 6420 cells from control animals and 2781 cells from the pulmonary hypertension model. Macrophages were classified

into M1 and M2 subsets using established markers (Il1b and Cd80 for M1; Cd163 and Mrc1 for M2). A modest elevation in M1 macrophage proportion was noted in the pulmonary hypertension group, rising from 23.6% to 30.0% **(Figures 5a–5c)**.

Along the pseudotime differentiation trajectory, M1-associated markers (Il1b and Cd80) increased while M2 markers (Cd163 and Mrc1) decreased in both conditions. Macrophages derived from pulmonary hypertension samples displayed a consistent bias toward the M1 state, in contrast to the more balanced distribution observed under normal conditions. This pattern underscores a disease-specific drive toward inflammatory macrophage polarization in the pulmonary hypertension setting **(Figure 5d)**.

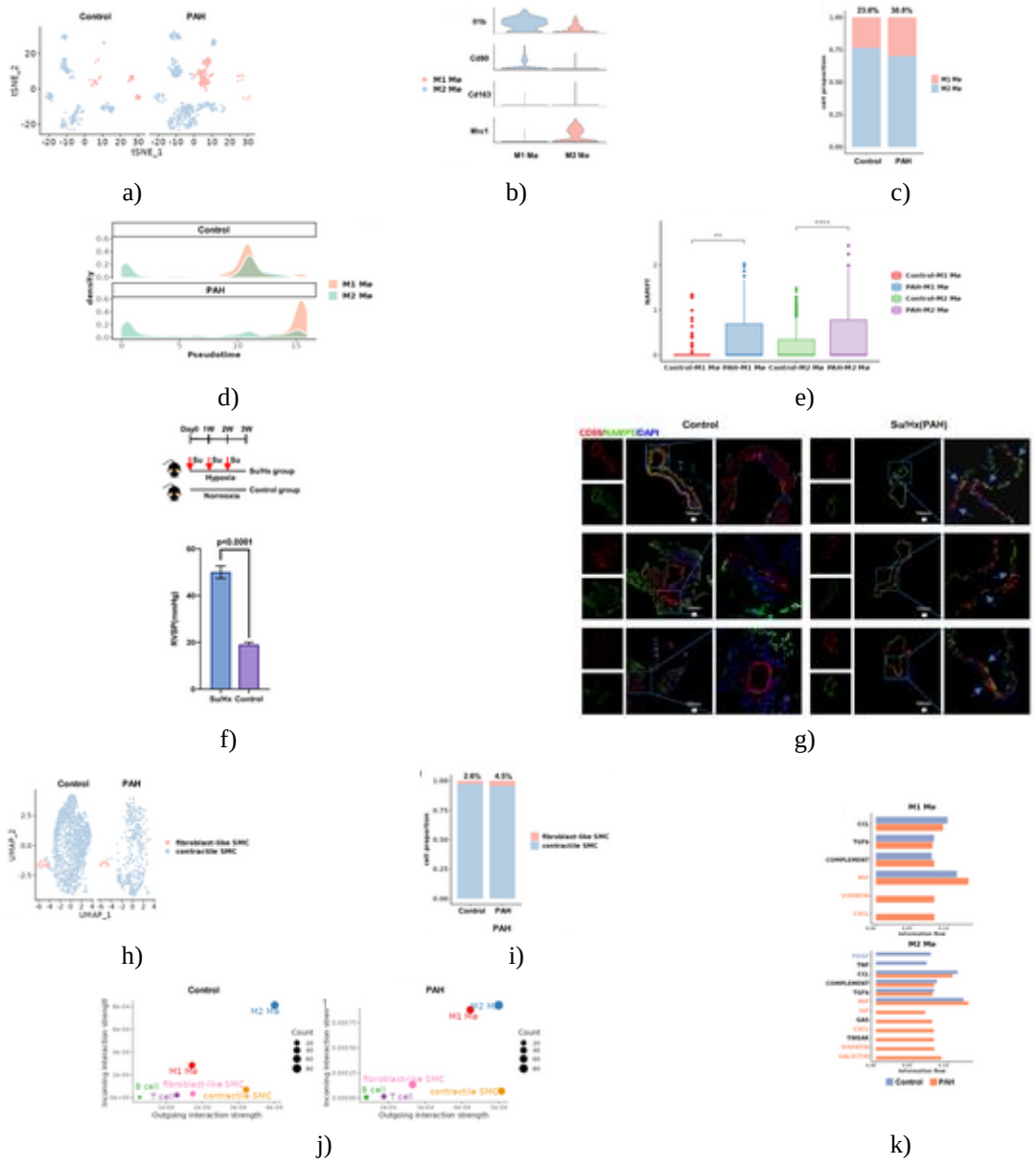

Figure 5. Macrophage NAMPT Upregulation Promotes M1 Polarization and Intensifies Macrophage-SMC Crosstalk in Mice.

(a) UMAP embeddings of reclustered macrophages derived from mouse pulmonary arterial cells, partitioned into distinct M1 and M2 subsets. (b) Violin plots showing the expression distribution of canonical macrophage marker genes (Il1b and Cd80 for the M1 subtype; Cd163 and Mrc1 for the M2 subtype). (c) Relative abundance of M1 and M2 macrophage subsets in control versus PAH samples. (d) Density distribution along the pseudotime axis for M1 and M2 macrophages under both control and disease conditions. (e) Direct comparison of Nampt transcript levels in macrophages between the two experimental groups. (f) Upper panel: schematic diagram of the sugen combined with hypoxia (Su/Hx) protocol for

inducing pulmonary hypertension in mice. Lower panel: quantitative evaluation of right ventricular systolic pressure (RVSP) across groups, with model validation performed via Student's t-test. (g) Immunofluorescence staining images revealing the co-localization of NAMPT protein with the macrophage marker CD68 in murine pulmonary arteries (scale bar, 100 μm). Higher-magnification insets of the blue-outlined regions demonstrate a substantial increase in NAMPT-positive macrophages in the PAH group. (h) UMAP visualizations of reclustered smooth muscle cells from mouse pulmonary arteries, subdivided into conventional contractile and fibroblast-like populations. (i) Comparative proportions of contractile versus fibroblast-like smooth muscle cells in control and PAH conditions. (j) Analysis of intercellular communication networks displaying interaction strengths among various cell types, emphasizing pronounced activation within M1 macrophages. (k) Bar graphs quantifying differences in outgoing signaling pathway activity for M1 and M2 macrophages between control and PAH states. RVSP, right ventricular systolic pressure; Su/Hx, sugen + hypoxia.

Additional analyses showed that Nampt transcript levels were elevated in both M1 and M2 macrophage populations in PAH samples compared with the control group **(Figure 5e)**. Trajectory analysis further demonstrated that rising Nampt expression correlated closely with the emergence of M1 macrophages. Of note, an early upregulation of Nampt was observed in M2 macrophages under PAH conditions, which may facilitate their transition toward an M1 phenotype.

The increase in macrophage NAMPT protein was independently validated through immunofluorescence staining in pulmonary arteries from mice exposed to the Sugen5416 (Su) plus hypoxia (Hx) model of PAH. Successful disease modeling was confirmed by elevated right ventricular systolic pressure **(Figures 5f and 5g)**.

To gain deeper insight into macrophage-SMC interactions in the disease setting, murine SMCs were extracted and classified according to established marker genes. Unlike their human counterparts, mouse SMCs consisted solely of contractile and fibroblast-like subtypes, with no evidence of a chondroid-like population. Nevertheless, the proportion of fibroblast-like SMCs increased under PAH conditions, paralleling findings in humans and reinforcing the conserved contribution of this subtype to pulmonary hypertension pathogenesis across species **(Figures 5h and 5i)**.

Intercellular communication profiling identified strong activation of M1 macrophage-SMC signaling in PAH, manifested as enhanced bidirectional interaction strengths. In comparison, other immune cell types such as T cells and B cells displayed only minor alterations **(Figure 5j)**. Consistent with prior observations, Nampt expression rose in both M1 and M2 macrophages during PAH **(Figure 5k)**, while SMCs showed heightened engagement of BMP and PROS signaling routes.

Overall, these results demonstrate that NAMPT-driven inflammatory polarization of macrophages augments their communication with SMCs undergoing phenotypic transition. The striking similarity to human findings highlights the broad relevance and robustness of NAMPT-mediated mechanisms in disease development.

Macrophage NAMPT-SMC CCR2/CCR5 axis governs fibroblast-like SMC phenotypic switching

To directly assess the influence of NAMPT on macrophage-SMC crosstalk and its consequences for SMC behavior, an in vitro transwell co-culture model was implemented. Murine peripheral blood macrophages were placed in the upper compartment and pulmonary arterial SMCs in the lower compartment, with NAMPT knockdown performed selectively in the macrophages **(Figure 6a)**. Effective suppression of NAMPT was confirmed using small interfering RNA **(Figure 6b)**. Evaluation of SMCs following this intervention revealed substantial downregulation of the phenotypic transition markers POSTN and RUNX2 **(Figures 6b, 6d and 6e)** as well as diminished migratory ability in transwell assays **(Figure 6c)**. These changes indicate that reducing NAMPT levels in macrophages limits the conversion of contractile SMCs into fibroblast-like cells. Remarkably, nearly all SMCs in the co-culture adopted a fibroblast-like appearance to some degree, emphasizing the powerful inductive effect exerted by macrophages **(Figure 6e)**.

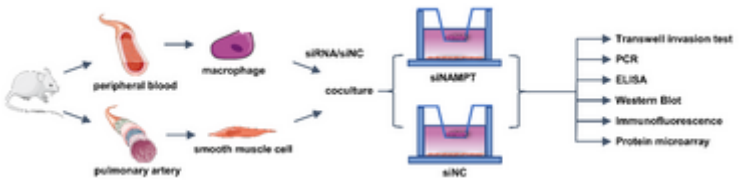

a)

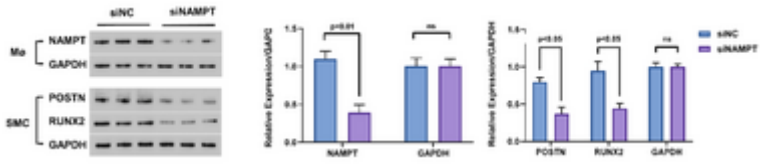

b)

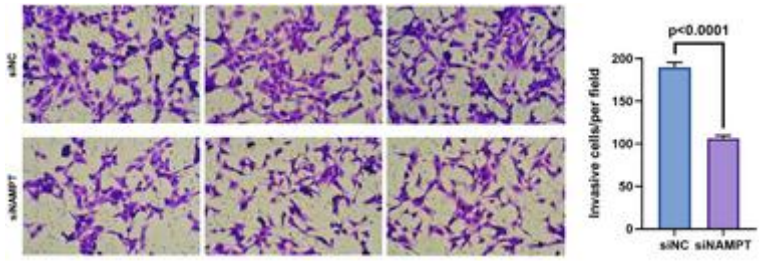

c)

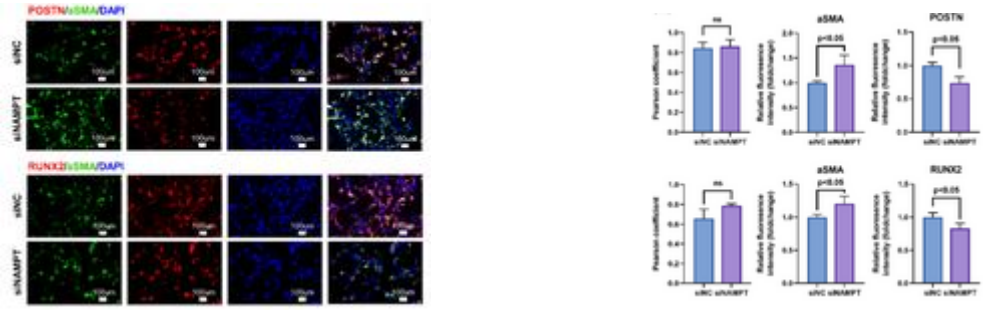

d) e)

Figure 6. NAMPT Suppression in Macrophages Attenuates SMC Phenotypic Transition. (a) Experimental workflow diagram depicting the transwell co-culture arrangement of murine peripheral blood-derived macrophages and pulmonary arterial smooth muscle cells, with or without targeted NAMPT interference, prior to subsequent functional assays. (b) Western blotting results for NAMPT protein abundance in macrophages following transfection with control siRNA (siNC) or NAMPT-specific siRNA (siNAMPT), together with levels of phenotypic modulation markers (POSTN and Runx2) in the co-cultured SMCs. Differences were evaluated statistically by Student's t-test. (c) Microscopic images of crystal violet-stained migrated cells (left panel) and the corresponding quantitative summary presented as a bar graph (right panel). Statistical analysis was conducted using Student's t-test. (d) Immunofluorescence micrographs illustrating the expression patterns of phenotypic switching markers RUNX2 and POSTN, in conjunction with the contractile marker aSMA, in SMCs (scale bar, 100 μm). (e) Measurement of Pearson's correlation coefficients and fluorescence intensity values for marker co-localization. Data represent the mean ± SD derived from three independent biological replicates, with statistical testing performed via Student's t-test. The figure was partly created with Servier Medical Art (http://smart.servier.com/), licensed under a Creative Commons Attribution 3.0 unported license.

To evaluate the influence of NAMPT on macrophage secretory activity, culture supernatants collected from control and NAMPT-deficient macrophages were subjected to protein microarray analysis. NAMPT knockdown resulted in reduced secretion of several cytokines, including IL1α, IL6, IFN-γ, TNF RI, and G-CSF, as well as chemokines such as MCP-1, MIP-1α, and MIG **(Figure 7a)**. These molecules are associated with pro-inflammatory functions, including cytokine activity, CCR chemokine receptor binding, response to chemokines, and cell chemotaxis **(Figure 7b)**. These observations further substantiate the role of NAMPT in driving M1 polarization of macrophages.

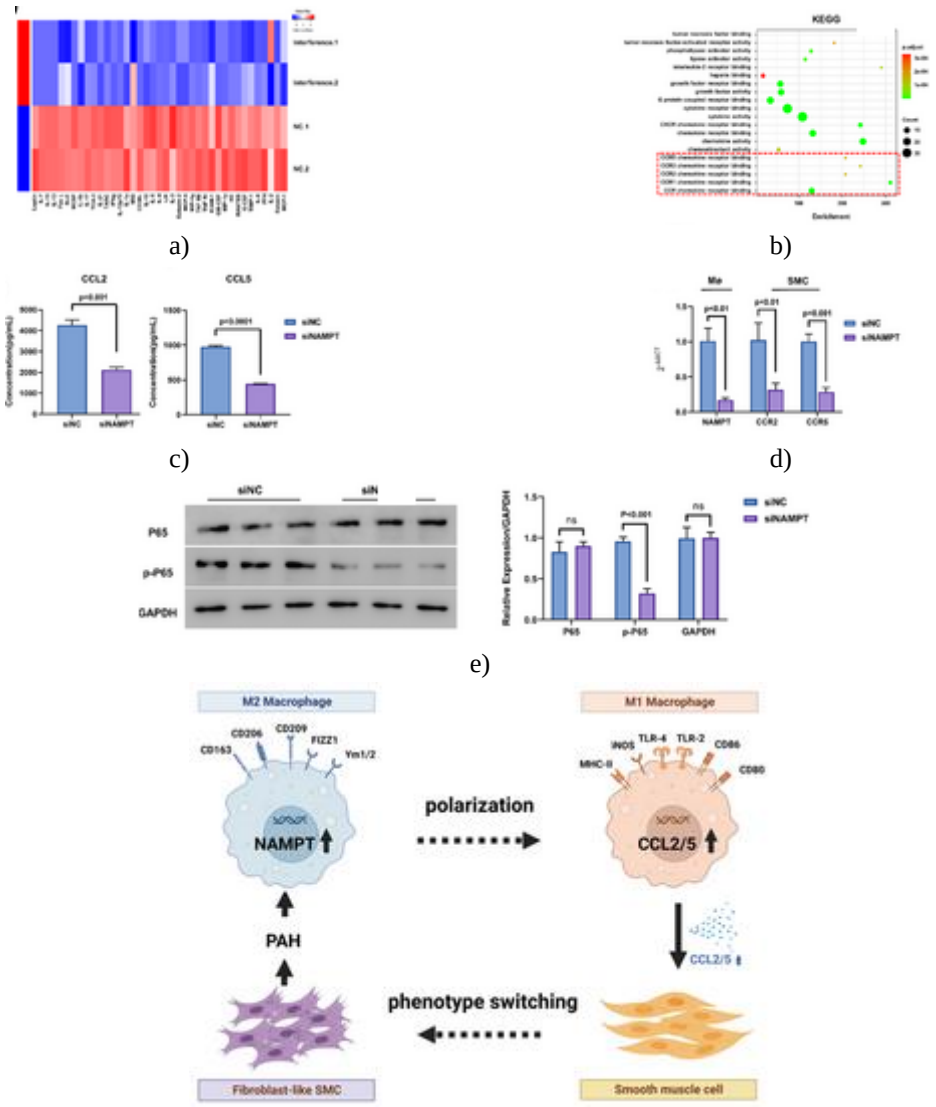

Figure 7. Inhibition of Macrophage Polarization through NAMPT Knockdown Impairs CCL2/5 Signaling to SMCs.

(a) Heatmap displaying the comparative secretion levels of chemokines and cytokines by macrophages in co-culture experiments treated with siNAMPT versus control siNC, as determined by protein array profiling. The color gradient indicates expression intensity from low (blue) to high (red). (b) Dot plot summarizing significantly enriched functional pathways identified from the protein array dataset. Dot diameter is proportional to the number of genes involved in each pathway, and dot color reflects the adjusted p-value (ranging from green for lower significance to red for higher significance). Pathways related to CCR signaling are enclosed in red dashed rectangles. (c) Bar chart presenting the mean ± SD levels of CCL2 and CCL5 detected in co-culture supernatants. (d) Bar chart showing relative expression of NAMPT in macrophages and CCR2/CCR5 in SMCs, normalized against GAPDH. Values represent mean ± SD of three independent replicates. Statistical differences were calculated using Student's t-test. (e) Western blotting results for total P65 and phosphorylated P65 protein abundance in smooth muscle cells under siNC and siNAMPT conditions. Quantitative analysis with statistical significance is provided in the adjacent panel. (f) Schematic representation of the proposed mechanism linking macrophage polarization to smooth muscle cell phenotypic modulation in pulmonary arterial hypertension.

Given the observed involvement of the CCR family following NAMPT interference **(Figure 7b)**, along with prior evidence suggesting that macrophages may influence SMC proliferation and migration through CCR2/CCR5 receptors in PAH [11, 23, 24], the study further examined the contribution of NAMPT to macrophage-SMC

interactions mediated by this chemokine axis. ELISA measurements demonstrated a substantial decrease in CCL2 and CCL5 secretion upon NAMPT knockdown **(Figure 7c)**. Consistent with this finding, qPCR analysis revealed marked downregulation of CCR2 and CCR5 expression in SMCs **(Figure 7d)**.

NF-κB signaling, which emerged as a recurrent pathway throughout the analyses **(Figure 3e)**, has also been implicated in CCL5-driven SMC phenotypic modulation [25]. In the present experiments, phosphorylation of P65—a key marker of NF-κB pathway activation—was significantly reduced in SMCs following NAMPT interference **(Figure 7e)**. This result supports the participation of NF-κB signaling in the NAMPT-dependent regulation of SMC phenotype.

In conclusion, under pathological conditions in PAH, macrophage-derived NAMPT enhances M1 polarization and stimulates the release of pro-inflammatory chemokines such as CCL2 and CCL5. These chemokines in turn promote fibroblast-like phenotypic switching in SMCs through activation of the CCR2/CCR5-NF-κB signaling cascade **(Figure 7f)**.

In this study, single-cell RNA sequencing was employed to construct a comprehensive cellular atlas of human pulmonary arteries. Three distinct phenotypic subsets of pulmonary arterial smooth muscle cells were identified: contractile, fibroblast-like, and chondroid-like. The analyses revealed that the shift from contractile to fibroblast-like SMCs is enhanced within the neointima in PAH. This transition is driven by intensified pro-inflammatory interactions with macrophages. Additionally, upregulation of NAMPT in macrophages was shown to alter their secretory profile. The abundance of NAMPT-expressing macrophages increased markedly in diseased pulmonary arteries, while targeted interference with NAMPT in macrophages reduced M1-like secretion and limited the fibroblast-like phenotypic transition of SMCs.

Excessive pulmonary vascular remodeling in the initial phases of PAH is largely driven by phenotypic modulation of SMCs, which involves heightened proliferation, migration, and invasive behavior [10]. However, the precise SMC subtype responsible for this remodeling has not been fully characterized. The present findings indicate that the fibroblast-like SMC phenotype serves as the predominant contributor to phenotypic switching in PAH, rather than the chondroid-like subtype. Accumulation of fibroblast-like SMCs in the neointima appears to play a significant role in lumen occlusion and the elevation of pulmonary pressure. Additional functional studies are necessary to clarify the precise contributions of fibroblast-like SMCs to PAH pathogenesis.

Macrophage polarization represents a dynamic response to microenvironmental cues. Accumulating evidence indicates a shift toward M1-dominant polarization in PAH patients [26, 27]. Multiple investigations have also highlighted the importance of enhanced macrophage-SMC interactions in promoting pathological SMC accumulation in PAH, attracting considerable research attention [11, 28, 29]. During early inflammatory responses, macrophages typically acquire an M1 phenotype and release pro-inflammatory mediators. Proper regulation is required to prevent excessive tissue injury, with a subsequent transition to M2 macrophages supporting resolution and repair [21, 30]. In atherosclerotic lesions, macrophages involved in apoptotic cell clearance secrete factors such as IL-10, TGF-β, and specialized pro-resolving mediators, which modulate SMC proliferation, migration, and matrix production, thereby stabilizing plaques [31]. In contrast, pro-inflammatory cytokines including IL1, IL6, and TNFα released by M1 macrophages exacerbate early thrombus formation and vessel narrowing in other vascular contexts [32].

The current results demonstrated an increased macrophage population and elevated M1/M2 ratio in PAH tissues, aligning with earlier reports linking M1/M2 imbalance to experimental pulmonary hypertension [27]. Targeting the pro-inflammatory microenvironment created by M1 macrophages may therefore represent a key strategy for reducing vascular remodeling in PAH. This is supported by the enrichment of pathways such as IL6-JAK-STAT3, IL2-STAT5, and TNFα. Experimental inhibition of JAK/STAT signaling has shown promising therapeutic potential in PAH [33]. Other M1-derived factors, including MMP1 and MMP10, have also been implicated in vascular remodeling processes [34].

Prior research has documented elevated NAMPT mRNA and protein levels in plasma, lung tissue, and pulmonary arterial endothelial cells from both patients and animal models of PAH. This elevation promotes SMC proliferation and phenotypic changes through enhanced store-operated calcium entry via Orai2 and STIM2, as well as paracrine-driven endothelial-to-mesenchymal transition [15, 35-37]. NAMPT exists in intracellular (iNAMPT) and extracellular (eNAMPT) forms. While iNAMPT primarily supports NAD biosynthesis inside cells, eNAMPT functions as a cytokine or adipokine influencing systemic metabolism and immunity [12]. Previous studies have shown that SOX- and HIF-2α-regulated eNAMPT secretion from pulmonary arterial endothelial cells stimulates SMC proliferation and EndMT, contributing to vascular remodeling [15, 16].

Macrophage-derived eNAMPT can sustain macrophage viability through IL-6/STAT3 signaling, generating a positive feedback loop [38]. Additionally, eNAMPT originating from perivascular adipose tissue exerts concentration- and time-dependent effects on SMC growth and confers protection against oxidative stress via ERK1/2 and p38 pathways [39].

In comparison, the role of iNAMPT in vascular disorders has received limited attention. It has been shown to influence differentiation and polarization of tumor-associated macrophages [40], with overexpression in bone marrow macrophages associated with decreased M1 characteristics [41]. In the present study, increased iNAMPT expression was observed in macrophages, consistent with patterns reported in other disease contexts. Silencing iNAMPT modified the macrophage secretory repertoire by lowering pro-inflammatory mediator release. This change weakened inflammatory crosstalk with SMCs and suppressed fibroblast-like phenotypic switching. Unlike the direct actions of eNAMPT on SMCs, iNAMPT appears to exert indirect effects on SMC behavior by shaping macrophage function and the surrounding inflammatory milieu. Interestingly, eNAMPT has been linked to M2 polarization in monocytes from chronic lymphocytic leukemia patients [42]. Whether this creates a counter-regulatory feedback loop with iNAMPT to stabilize macrophage phenotypes merits further exploration.

Several limitations should be acknowledged. The precise molecular pathways connecting NAMPT-mediated macrophage polarization to SMC phenotypic switching require additional clarification, particularly through in vivo models. The influence of iNAMPT on other vascular processes, such as EndMT, also warrants investigation.

Conclusion

In summary, the present work provides important insights into the cellular and molecular basis of PAH. It underscores the contribution of NAMPT-driven macrophage polarization to fibroblast-like phenotypic switching in SMCs and positions iNAMPT as a potential therapeutic target for reducing vascular remodeling and disease severity in pulmonary arterial hypertension.

Acknowledgments: None

Conflict of Interest: None

Financial Support: None

Ethics Statement: None

References

1. Ruopp NF, Cockrill BA. Diagnosis and Treatment of Pulmonary Arterial Hypertension: A Review. JAMA. 2022;327(14):1379-91.
2. Zhong L, Leng S, Alabed S, Chai P, Teo L, Ruan W, et al. Machine Learning-Based Three-Dimensional Echocardiographic Evaluation of Right Ventricular Size and Function in Pulmonary Hypertension. JACC Cardiovasc Imaging. 2023;16(8):1022-34.
3. Hassoun PM. Pulmonary Arterial Hypertension. N Engl J Med. 2021;385(25):2361-76.
4. Thompson AAR, Lawrie A. Targeting Vascular Remodeling to Treat Pulmonary Arterial Hypertension. Trends Mol Med. 2017;23(1):31-45.
5. Hoeper MM, Humbert M, Souza R, Idrees M, Kawut SM, Sliwa-Hahnle K, et al. A global view of pulmonary hypertension. Lancet Respir Med. 2016;4(4):306-22.
6. Stenmark KR, Frid MG, Graham BB, Tuder RM. Dynamic and diverse changes in the functional properties of vascular smooth muscle cells in pulmonary hypertension. Cardiovasc Res. 2018;114(4):551-64.
7. Chakraborty R, Chatterjee P, Dave JM, Ostriker AC, Greif DM, Rzucidlo EM, et al. Targeting smooth muscle cell phenotypic switching in vascular disease. JVS-Vasc Sci. 2021;2:79-94.
8. Chen X, Wei X, Ma S, Xie H, Huang S, Yao M, et al. TREM-1 promotes pulmonary arterial hypertension by inducing macrophage polarization and vascular remodeling. Toxicol Appl Pharmacol. 2022;457:116319.
9. Lechartier B, Berrebeh N, Huertas A, Humbert M, Guignabert C, Tu L. Phenotypic Diversity of Vascular Smooth Muscle Cells in Pulmonary Arterial Hypertension: Implications for Therapy. Chest. 2022;161(1):219-31.

10. Ma B, Cao Y, Qin J, Chen Z, Hu G, Li Q. Macrophage polarization in pulmonary arterial hypertension: therapeutic implications. Drug Discov Today. 2023;28(6):103559.
11. Abid S, Marcos E, Parpaleix A, Amsellem V, Breau M, Houssaini A, et al. Telomere dysfunction in pulmonary arterial hypertension. Eur Respir J. 2019;54(6):1802308.
12. Dahl TB, Holm S, Aukrust P, Halvorsen B. Vessel wall biology and inflammation in pulmonary arterial hypertension. Annu Rev Nutr. 2012;32:229-52.
13. Zhou L, Zhang S, Bolor-Erdene E, Wang L, Tian D, Mei Y. The Role of Macrophage Polarization in Pulmonary Arterial Hypertension. Oxid Med Cell Longev. 2020;2020:1974265.
14. Dakroub A, Nasser SA, Kobeissy F, Yassine HM, Orekhov A, Sharifi-Rad J, et al. Macrophage polarization in cardiovascular diseases. J Cell Physiol. 2021;236(9):6282-301.
15. Chen J, Sysol JR, Singla S, Zhao S, Yamamura A, Valdez-Jasso D, et al. Nicotinamide Phosphoribosyltransferase Promotes Pulmonary Vascular Remodeling and Is a Therapeutic Target in Pulmonary Arterial Hypertension. Circulation. 2017;135(16):1532-46.
16. Wu Y, Wharton J, Walters R, Vasilaki E, Aman J, Zhao L, et al. The role of macrophages in pulmonary arterial hypertension. Eur Respir J. 2021;58(4):2004172.
17. Asosingh K, Comhair S, Mavrakis L, Xu W, Horton D, Taylor I, et al. Pulmonary vascular remodeling in pulmonary hypertension: role of macrophages. Sci Rep. 2021;11(1):14714.
18. Crnkovic S, Valzano F, Fließer E, Gindlhuber J, Thekkekara Puthenparampil H, Basil M, et al. Single-cell transcriptomics reveals skewed cellular communication and metabolic reprogramming in pulmonary hypertension. JCI Insight. 2022;7(16):e153471.
19. Corcoran L, Emslie D, Kratina T, Shi W, Hirsch S, Taubenheim N, et al. The role of macrophages in pulmonary hypertension. Front Immunol. 2014;5:108.
20. Hu Z, Zhao TV, Huang T, Ohtsuki S, Jin K, Goronzy IN, et al. TREM-1 and TREM-2 in pulmonary hypertension. Nat Metab. 2022;4(6):759-76.
21. Shapouri-Moghaddam A, Mohammadian S, Vazini H, Taghadosi M, Esmaeili SA, Mardani F, et al. Macrophage plasticity, polarization, and function in health and disease. J Cell Physiol. 2018;233(9):6425-40.
22. Sun Y, Wu L, Zhong Y, Zhou K, Hou Y, Wang Z, et al. Single-cell landscape of the ecosystem in early-onset colorectal cancer. Cell. 2021;184(2):404-20.
23. Amsellem V, Lipskaia L, Abid S, Poupel L, Houssaini A, Quarck R, et al. Telomere dysfunction causes sustained inflammation and induces severe pulmonary hypertension. Circulation. 2014;130(15):1306-18.
24. Amsellem V, Abid S, Poupel L, Parpaleix A, Rodero M, Gary-Bobo G, et al. CX3CR1+ Macrophages Promote Pulmonary Hypertension. Am J Respir Cell Mol Biol. 2017;56(5):597-608.
25. Lin CS, Hsieh PS, Hwang LL, Lee YH, Tsai SH, Tu YC, et al. Macrophage Polarization and Pulmonary Hypertension. Cell Physiol Biochem. 2018;47(2):707-21.
26. Hashimoto-Kataoka T, Hosen N, Sonobe T, Arita Y, Yasui T, Masaki T, et al. Interleukin-6/interleukin-21 signaling axis is critical for the development of pulmonary arterial hypertension. Proc Natl Acad Sci USA. 2015;112(20):E2677-86.
27. Zawia A, Arnold ND, West L, Pickworth JA, Turton H, Iremonger J, et al. Macrophage-Derived IL-1β Promotes Pulmonary Vascular Remodeling. Arterioscler Thromb Vasc Biol. 2021;41(1):430-44.
28. Koga J, Aikawa M. Macrophage plasticity and polarization in vascular disease. Vasc Pharmacol. 2012;57(1):24-32.
29. Ntokou A, Dave JM, Kauffman AC, Sauler M, Ryu C, Hwa J, et al. Macrophage-derived Wnt ligands promote vascular smooth muscle cell proliferation in pulmonary hypertension. JCI Insight. 2021;6(16):e139067.
30. Wculek SK, Dunphy G, Heras-Murillo I, Mastrangelo A, Sancho D. Metabolism of tissue macrophages in homeostasis and pathology. Cell Mol Immunol. 2022;19(3):384-99.
31. Yurdagul A. Metabolic Reprogramming of Macrophages in Pulmonary Hypertension. Arterioscler Thromb Vasc Biol. 2022;42(4):372-88.
32. Rai V, Singh H, Agrawal DK. Macrophage Polarization in Pulmonary Arterial Hypertension. Int J Mol Sci. 2022;23(19):12012.
33. Yerabolu D, Weiss A, Kojonazarov B, Boehm M, Schlueter BC, Ruppert C, et al. Targeting macrophages in pulmonary arterial hypertension. Am J Respir Cell Mol Biol. 2021;64(1):100-18.
34. Chi PL, Cheng CC, Hung CC, Wang MT, Liu HY, Ke MW, et al. Macrophage polarization and vascular inflammation in pulmonary hypertension. Int J Biol Sci. 2022;18(1):331-47.

35. van der Veer E, Ho C, O'Neil C, Barbosa N, Scott R, Cregan SP, et al. Smooth muscle cell phenotype switching and vascular disease. J Biol Chem. 2007;282(15):10841-51.
36. Borradaile NM, Pickering JG. Nicotinamide phosphoribosyltransferase and vascular smooth muscle cell senescence. Aging Cell. 2009;8(2):100-12.
37. Sun X, Sun BL, Babicheva A, Vanderpool R, Oita RC, Casanova N, et al. Macrophage-derived exosomes promote pulmonary vascular remodeling. Am J Respir Cell Mol Biol. 2020;63(1):92-105.
38. Li Y, Zhang Y, Dorweiler B, Cui D, Wang T, Woo CW, et al. Nicotinamide phosphoribosyltransferase and macrophage function. J Biol Chem. 2008;283(50):34833-43.
39. Wang P, Li WL, Liu JM, Miao CY. Macrophage polarization in vascular disease. J Cardiovasc Pharmacol. 2016;67(6):474-82.
40. Sica A, Strauss L, Consonni FM, Travelli C, Genazzani A, Porta C. Metabolic regulation of macrophage polarization. Cytokine Growth Factor Rev. 2017;35:27-36.
41. Bermudez B, Dahl TB, Medina I, Groeneweg M, Holm S, Montserrat-de la Paz S, et al. Macrophage polarization and lipid metabolism in vascular disease. Arterioscler Thromb Vasc Biol. 2017;37(6):1157-68.
42. Audrito V, Serra S, Brusa D, Mazzola F, Arruga F, Vaisitti T, et al. Nicotinamide phosphoribosyltransferase and T-cell function. Blood. 2015;125(1):111-9.